Chemical Geology 611 (2022) 121089

Contents lists available at ScienceDirect

Chemical Geology

journal homepage: www.elsevier.com/locate/chemgeo

On the nucleation of ikaite ($CaCO_3x6H_2O$) – A comparative study in the presence and absence of mineral surfaces

Samuel B. Strohm [a], Sebastian E. Inckemann [a], Kun Gao [a], Michael Schweikert [b,c], Marie-Louise Lemloh [c,d], Wolfgang W. Schmahl [a], Guntram Jordan [a,*]

[a] Department für Geo- und Umweltwissenschaften (Sektion Kristallographie), Ludwig-Maximilians-Universität München, Theresienstraße 41, 80333 München, Germany
[b] Institute of Biomaterials and Biomolecular Systems, Biobased Materials Group, Universität Stuttgart, Pfaffenwaldring 57, 70569 Stuttgart, Germany
[c] AMICA – Stuttgart Research Focus (SRF), Universität Stuttgart, Pfaffenwaldring 32, 70569 Stuttgart, Germany
[d] Materials Testing Institute (MPA), Universität Stuttgart, Pfaffenwaldring 32, 70569 Stuttgart, Germany

ARTICLE INFO

Editor name: Michael E. Boettcher

Keywords:
Ikaite
Heterogeneous nucleation
Non-classical nucleation
ACC
Surfaces
Hydrous carbonate minerals

ABSTRACT

The formation of ikaite ($CaCO_3x6H_2O$) was studied in the presence and absence of quartz and mica surfaces using desupersaturation curves from cryo-mixed-batch-reactor experiments. Upon nucleation and growth within the reactor, the solution approached solubility of the precipitating carbonate phase. For ikaite, a solubility constant of $\log K_{sp\ \mathrm{ikaite}} = -7.3 \pm 0.1$ was found ($T = 0$ °C). At supersaturations $\Omega_{\mathrm{ikaite}} < 15$, the nucleation of ikaite was significantly promoted by the presence of quartz or mica. This promotion prevented a competing nucleation of anhydrous calcium carbonates. In the presence of quartz or mica, therefore, ikaite forms over a much broader supersaturation range than in the absence. Similarly strong promotors of ikaite nucleation rather than anhydrous carbonate nucleation were previously attributed to calcite-inhibiting substances only.

At supersaturations $\Omega_{\mathrm{ikaite}} \geq 8$, application of classical nucleation theory on induction periods of ikaite formation yielded an effective interfacial energy of 15 ± 3 mJ/m^2. Compared to data of anhydrous $CaCO_3$ phases, this interfacial energy is low and expresses the highly hydrated character of ikaite. At supersaturations $\Omega_{\mathrm{ikaite}} \geq 18$, a transient amorphous phase appeared besides ikaite.

Our results show that a comprehensive understanding of ikaite formation in natural settings requires consideration not only of supersaturation and presence of calcite-inhibitors but also of the presence or absence of mineral surfaces capable of promoting heterogeneous nucleation of ikaite.

1. Introduction

Calcium carbonate minerals are ubiquitous on Earth's surface. The minerals are important parts of the global carbon cycle and, therefore, significantly affect the physicochemical conditions on Earth (e.g., Martin, 2017; Millero, 2007; Ridgwell and Zeebe, 2005). The crystallization pathways of carbonate minerals are complex and often include intermediate phases that essentially affect the selection and properties of the final anhydrous phase (Besselink et al., 2017; Blue et al., 2017; Gebauer et al., 2014). Nucleation and transformation of these intermediate hydrous crystalline and amorphous calcium carbonates, therefore, are subject to numerous recent studies (Besselink et al., 2017; Blue et al., 2017; Cartwright et al., 2012; Chaka, 2018; Gebauer and Cölfen, 2011; Radha et al., 2010; Rodriguez-Blanco et al., 2011; Rodríguez-Ruiz et al., 2014). One of the most challenging calcium carbonate minerals is ikaite ($CaCO_3x6H_2O$) due to the low stability of its crystal structure, which is composed of a hydrogen bond network connecting $CaCO_3^0$ ion pairs (Demichelis et al., 2014; Dickens and Brown, 1970; Hesse et al., 1983). This weak hydrogen bond network readily allows for water diffusion and dehydration (Chaka, 2018; Zaoui and Sekkal, 2014). Consequently, ikaite mainly appears as a transient phase transforming to more stable anhydrous calcium carbonates (Besselink et al., 2017; Purgstaller et al., 2017; Sánchez-Pastor et al., 2016; Tang et al., 2009) or amorphous calcium carbonate (Zou et al., 2018).

Although ikaite is more soluble than anhydrous calcium carbonate minerals and, therefore, is metastable at Earth's surface conditions (Marland, 1975), widespread occurrences of ikaite and pseudomorphs after ikaite (*glendonites*) were reported especially from cold environments (Bischoff et al., 1993b; Boch et al., 2015; Council and Bennett, 1993; Ito, 1996; Jansen et al., 1987; Lu et al., 2012; Oehlerich et al.,

* Corresponding author.
E-mail address: jordan@lmu.de (G. Jordan).

https://doi.org/10.1016/j.chemgeo.2022.121089
Received 22 July 2022; Received in revised form 25 August 2022; Accepted 27 August 2022
Available online 3 September 2022

2013; Omelon et al., 2001; Pauly, 1963; Shearman and Smith, 1985; Suess et al., 1982). Noteworthy, ikaite also was identified within sea ice, where it might play an important role in the polar carbon cycles (Dieckmann et al., 2008; Dieckmann et al., 2010; Fischer et al., 2013; Geilfus et al., 2013). The discrepancy between frequent occurrence in nature and metastability led to many studies investigating the physicochemical conditions which promote the formation of ikaite over anhydrous $CaCO_3$-minerals. These studies showed that the formation of ikaite is especially supported by factors ensuring a sufficiently high supersaturation: elevated alkalinity (Bischoff et al., 1993a), alkaline solution conditions (Boch et al., 2015; Hu et al., 2015), and cold (but not necessarily near-freezing) temperatures (Johnston et al., 1916; Stockmann et al., 2018; Tollefsen et al., 2020). Ikaite formation can further be induced by the presence of substances selectively inhibiting a competing calcite precipitation, notably aqueous Mg^{2+} and phosphate (Bischoff et al., 1993a; Buchardt et al., 2001; Hu et al., 2014; Stockmann et al., 2018; Tollefsen et al., 2018). Despite the pronounced efficiency of these inhibitors, the presence of such substances is not a prerequisite for ikaite formation as various experimental studies at cold solution temperatures have been demonstrating (Besselink et al., 2017; Boch et al., 2015; Hu et al., 2015; Johnston et al., 1916; Zou et al., 2018).

Even though the number of studies on ikaite formation is large, the physicochemical conditions leading to ikaite rather than anhydrous carbonates are still poorly constrained. One reason is that conditions which promote ikaite formation, may concurrently lead to a more rapid transformation of ikaite into more stable $CaCO_3$-minerals. If the time span of ikaite existence falls below temporal resolution of experiments, the occurrence of ikaite as a transient precursor of anhydrous carbonate minerals may remain unnoticed. Moreover, the mechanisms of ikaite formation were subject to only few studies and, therefore, are largely unknown as well. From experiments in highly supersaturated solutions, Besselink et al. (2017) and Zou et al. (2018) reported an onset of ikaite precipitation during dissolution of a previously formed amorphous calcium carbonate precursor. Important to note, that the amorphous precursor is supposed to contain an amount of water similar to ikaite (Zou et al., 2018).

In precipitation experiments conducted with Mg-rich solution at 6 and 12 °C, Purgstaller et al. (2017) did not reveal a highly hydrated precursor and suggested that the precipitation of ikaite rather than anhydrous calcium carbonates is linked to the slow dehydration kinetics of Ca^{2+} species at near-freezing temperatures. The expendability of a complete dehydration of aqueous Ca^{2+} for ikaite formation was also implied by Buchardt et al. (2001) and Stockmann et al. (2018). These authors concluded from ikaite precipitation in sea water at cold temperatures ($\leq$ 15 °C) that an increased activity of the $CaCO_3^0$ ion pair species in solution could play a key role for the formation of ikaite. Further corroboration comes from DFT-calculations (Chaka, 2018) which assign a decisive role to the aqueous $CaCO_3x6H_2O$ complexes for ikaite nucleation. Chaka (2018) showed a close structural correspondence between the aqueous $CaCO_3x6H_2O$ ion pair complexes and the $CaCO_3x6H_2O$ structure unit within the ikaite crystal lattice. Hence, if a mere self-organization of aqueous ion pair complexes may lead to nucleation, this could provide a low energy pathway of ikaite formation (Chaka, 2018).

Ikaite nucleation has been studied in (pseudo-)homogeneous cases (volume nucleation) so far, except for the influence of polymer surfaces functionalized with nitrile groups (Malkaj et al., 2002). Foreign substrates like mineral surfaces, however, are ubiquitous in natural precipitation settings. These mineral surfaces could affect ikaite formation significantly. According to the classical perspective on mineralization, the nucleation barrier can be reduced, if a phase nucleates on mineral substrates (e.g., De Yoreo et al., 2013; Kashchiev and van Rosmalen, 2003; Mullin, 2001; Sangwal, 2007). Mineral substrates, therefore, can significantly promote the formation of a phase. For calcite, it has been shown that nucleation on substrates with carboxyl groups follows the classical perspective (Hu et al., 2012). Furthermore, a study using substrates with carboxyl, thiol, phosphate, and hydroxyl groups yielded a correlation of the nucleation rate with the lattice match between calcite and substrate (Hamm et al., 2014). On mica substrates, moreover, vaterite formation was larger than calcite formation, whereas the total carbonate formation on mica was more extensive than on quartz surfaces (Li et al., 2014).

For the formation of anhydrous calcium carbonate minerals, these studies confirm a substrate induced promotion. Such a promotion, however, does not need to take place in case of all minerals on all substrates at all conditions. Particularly as promotion of the formation of anhydrous calcium carbonates may take place via a favoured dehydration of ions and/or ion pairs at the mineral substrates, this effect cannot directly be transferred to ikaite nucleation as the constituent structural units of ikaite may correspond to the hydrated $CaCO_3^0$ ion pairs in solution. In contrast to other factors promoting ikaite formation (such as alkalinity, temperature, or calcite inhibiting additives), the role of minerals surfaces, although ubiquitous in all natural ikaite formation settings, is largely unexplored. Aim of this study, therefore, is to provide a contribution for a better understanding of ikaite formation in natural settings by investigating ikaite formation in presence and absence of quartz and mica substrates as proxies for common natural minerals.

2. Methods

2.1. Materials

Experiments were performed using solutions which were prepared by dissolving analytical-grade chemicals ($CaCl_2x2H_20$, Na_2CO_3, $NaHCO_3$) in deionized water with a resistivity of 18.2 MΩ cm and adjusting ionic strength and solution pH using NaCl and NaOH, respectively. Quartz substrates were prepared by grinding quartz powder from *Fluka*. Mica substrates (*Ziegler Minerals*, Germany, particle size <45 μm, chemical composition: SiO_2: 46%, Al_2O_3: 32%, K_2O: 11%, Fe_2O_3 < 5%, Na_2O_3: 0.3%, MgO: 0.2%, TiO_2: 0.6%) were utilized without grinding. The powders were washed and decanted with deionized water (18.2 MΩ cm) several times. Specific surface areas of 0.21 m^2/g for quartz and 3.97 m^2/g for mica substrates were determined by krypton gas adsorption following standard BET procedures.

2.2. Cryo-mixed-batch-reactor experiments

Precipitation experiments were carried out in a cryo-mixed-batch-reactor (CMBR; total reactor volume: 250 ml) submerged in a

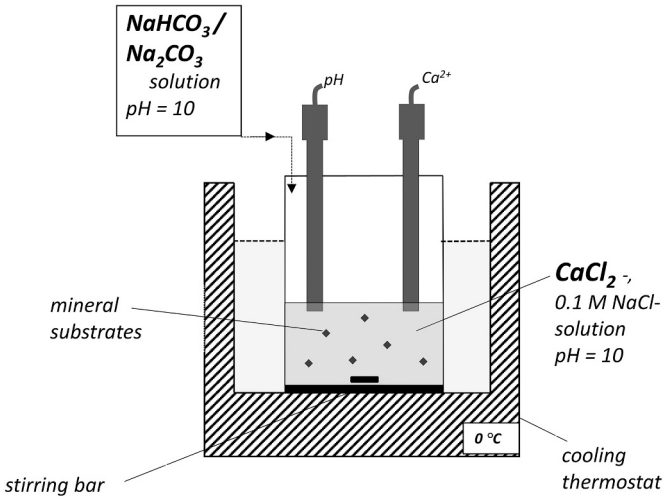

Fig. 1. Experimental set up of a cryo-mixed-batch-reactor (CMBR) experiment. Ca^{2+}- and HCO_3^-/CO_3^{2-}-containing solutions were mixed in the reactor in presence or absence of mineral substrates (quartz, mica).

thermostatic water bath (Lauda Alpha RA 8) (Fig. 1). The $CaCl_2$ solution (ionic strength = 0.1 M, pH = 10) was filled into the reactor under stirring at 0 °C. Quartz crystals were added to the reactor in one series of experiments and mica in a second series. In a third series aiming at pseudohomogeneous ikaite formation, no substrate crystals were added. Upon addition of the substrate crystals, in situ monitoring of solution pH and Ca^{2+} concentration was started using a standard glass electrode (calibrated with NIST certified pH 4.01, 7.13 and 10.32 buffer solutions at 0 °C) and a Ca^{2+}-ion-selective electrode, respectively, with a multi-parameter benchtop meter (HANNA instruments HI 5222). Subsequently, $NaHCO_3/Na_2CO_3$ solution was added instantaneously to the reactor leading to a total solution volume of 200 ml. Rigorous stirring by a magnetic stirrer allowed mixing of the solutions within the reactor in <5 s. For each condition (Table 1), experiments were performed in triplicate. Upon the end of the experiment, the solids (substrates and precipitates) were separated from the solution by vacuum filtration, rapidly washed with ethanol ($T = -18$ °C) and stored in a freezer (−18 °C) for further analyses as described below. The entire process of retrieval and washing was accomplished within <30 s.

2.3. Phase analysis by X-ray powder diffraction

The cooled solid samples from CMBR experiments were analyzed by X-ray powder diffraction (GE Seifert, CuKα_1 radiation, $\lambda = 1.5406$ Å) with scattering angels of $10° \leq 2\theta \leq 60°$. Sample holders were precooled (−18 °C). Routine analyses were conducted within <12 min in order to avoid temperature-induced phase transitions during measurement. Faster scans ($12° \leq 2\theta \leq 35°$, 3 min) were used to inspect the samples for highly instable phases.

2.4. Cryo scanning electron microscopy (cryo SEM)

Cryo SEM (Zeiss EVO 15 equipped with a cool stage) was used to image solid samples retrieved from the CMBR experiments. The samples were visualised using secondary electrons and back-scattered electrons with an Everhart-Thornley detector. An acceleration voltage of 20 kV was used. The cool stage was set to $T = -25$ °C.

2.5. Solution analysis

Samples of the filtered solution from CMBR experiments were analyzed by titration. Ca^{2+} concentrations and total alkalinity were both analyzed by potentiometric end point titrations using a SI Instruments Titroline 7000. Total alkalinity was determined using a standard glass electrode calibrated with NIST certified pH 4.01, 7.01 and 10.01 buffer solutions and 0.01 M HCl standard solution (detection limit: 2×10^{-5} M). Ca^{2+} concentrations were analyzed using 0.01 M Na_2-EDTA standard solution and a Ca^{2+} ion selective electrode (Ca^{2+}-ISE) with a detection limit of 2×10^{-5} M.

Solution compositions, speciations and saturations were modelled with the geochemical modelling program PHREEQC version 3.7.0 (Parkhurst and Appelo, 2013). All simulations were performed using the llnl database. Solubility constants of ikaite (log $K_{sp} = 0.15981–2011.1/T$, Bischoff et al., 1993a), vaterite (log $K_{sp} = -172.1295–0.077993\ T + 3074.688/T + 71.595 \log T$, Plummer and Busenberg, 1982), ACC (log $K_{sp} = -12.9185287 + 0.05453848\ T - 0.0001096\ T^2$, Brečević and Nielsen, 1989) were added to the database. The saturation state Ω was defined as

$$\Omega = \frac{IAP}{K_{sp}} \tag{1}$$

where IAP is the ionic activity product in the aqueous solution and K_{sp} is the solubility product of the solid.

2.6. Induction periods (t_{ind}) and interfacial energies (γ)

Ca^{2+} and pH monitoring of solution in CMBR experiments was applied to evaluate the induction period t_{ind} of precipitation. t_{ind} is defined by the interval between attaining a supersaturated solution and the growth of nuclei to a detectable size causing a measurable change of pH or Ca^{2+} signal (Gómez-Morales et al., 1996; Söhnel and Mullin, 1988). In our experiments, the induction period was defined as the period between creating a supersaturated solution by adding carbonate to the Ca^{2+} solution within the reactor and the first decrease of the pH/Ca^{2+} signals detectable by pH and Ca^{2+} monitoring (Fig. 2). In order to determine t_{ind}, we used the inflection of the first derivative of a polynomial fit of our experimental data. Induction periods determined by pH monitoring generally agreed well with t_{ind} indicated by Ca^{2+} measurements. However, at our experimental conditions including cold temperatures of 0 °C, pH monitoring provided more precise data compared to Ca^{2+} measurements. Due to the dynamics of the nucleation process involving decreasing pH-values, the Ca^{2+}-ISE cannot be calibrated with sufficient precision. Hence, all induction periods as well as the calculations based on these t_{ind}-data resulted from pH monitoring.

For the use of the induction period t_{ind} as a measure of the nucleation process, the simplifying assumption is required that for a constant solution volume (=200 ml) t_{ind} can be expressed as the reciprocal of the nucleation rate J (Söhnel and Mullin, 1988):

$$t_{ind} = J^{-1} \tag{2}$$

where J can be defined by classical nucleation theory (CNT) as

$$J = A \quad exp\left[-\frac{\beta\gamma^3 V_m^2 f(\theta) N_A}{\nu^2 (RT)^3 ln^2 \Omega}\right] \tag{3}$$

with A: kinetic pre-factor, β: shape factor ($16\pi/3$ for a spherical nucleus), V_m: molecular volume (114 cm^3/mol for ikaite), $f(\theta)$: correction factor ($f(\theta) = 1$ for homogeneous nucleation and $f(\theta) < 1$ for heterogeneous nucleation), N_A: Avogadro number, ν^2: number of ions in a molecular unit($\nu = 2$ for ikaite), R: gas constant, T: temperature (Mullin, 2001; Söhnel and Mullin, 1988). The rearranged combination of eqs. (2) and (3) give

$$log t_{ind} = \frac{B}{log^2 \Omega} - C \tag{4}$$

with

$$C = log \quad A \tag{5}$$

and

$$B = \frac{\beta\gamma^3 V_m^2 f(\theta) N_A}{\nu^2 (2.3RT)^3} \tag{6}$$

Obviously, the parameter B corresponds to the slope when log t_{ind} is plotted against $(\log \Omega)^{-2}$ at constant temperature. The slope B, therefore, yields the interfacial energy γ (Mullin, 2001; Söhnel and Mullin, 1988).

3. Results

3.1. Precipitated phases

In all CMBR experiments, at least one phase precipitated from supersaturated solution

(Table 1). Ikaite, however, did not crystallize under all conditions. In absence of mineral substrates, ikaite only formed in solutions with an initial supersaturation Ω_{ikaite} of at least 15 (Table 1, exp. # 16, 19, 22, 25), whereas in solutions with lower Ω_{ikaite}, calcite and vaterite could be identified (Fig. 3A). In presence of 0.5 g quartz or 0.1 g mica substrates,

Table 1
Precipitates and induction periods of formation as a function of solution conditions. Activities and supersaturations (Ω) were calculated using PHREEQC (Parkhurst and Appelo, 2013) and correspond to the initial state of mixed solutions.

Experiment		Solution speciation[a]					Saturation[a]					Precipitates and t_{ind}	
Exp no	Substrate	pH	a^{2+}_{Ca} [mM]	a^{-}_{HCO3} [mM]	a^{2-}_{CO3} [mM]	a^{0}_{CaCO3} [mM]	Ω_{ikaite}	$\log^{-2}\Omega_{ikaite}$	Ω_{CC}[b]	Ω_{VA}[b]	Ω_{ACC}[b]	Phase[b]	t_{ind} [s]
1.1	none	10.18	0.55	0.52	0.19	0.13	1.6	24	25	6	0.16	CC, VA	15,470
1.2	none	″	″	″	″	″	″	″	″	″	″	CC, VA	10,220
1.3	none	″	″	″	″	″	″	″	″	″	″	CC	18,370
2.1	0.5 g quartz	″	″	″	″	″	″	″	″	″	″	IK	6765
2.2	0.5 g quartz	″	″	″	″	″	″	″	″	″	″	IK	9365
2.3	0.5 g quartz	″	″	″	″	″	″	″	″	″	″	IK	11,365
3.1	0.1 g mica	″	″	″	″	″	″	″	″	″	″	IK	3485
3.2	0.1 g mica	″	″	″	″	″	″	″	″	″	″	IK	2365
3.3	0.1 g mica	″	″	″	″	″	″	″	″	″	″	IK	3110
4.1	none	10.16	0.71	0.68	0.23	0.21	2.6	6	41	9	0.26	CC, VA	3585
4.2	none	″	″	″	″	″	″	″	″	″	″	CC, VA	3240
4.3	none	″	″	″	″	″	″	″	″	″	″	CC, VA	3360
5.1	0.5 g quartz	″	″	″	″	″	″	″	″	″	″	IK	1222
5.2	0.5 g quartz	″	″	″	″	″	″	″	″	″	″″	IK	589
5.3	0.5 g quartz	″	″	″	″	″	″	″	″	″	″	IK	440
6.1	0.1 g mica	″	″	″	″	″	″	″	″	″	″	IK	420
6.2	0.1 g mica	″	″	″	″	″	″	″	″	″	″	IK	433
6.3	0.1 g mica	″	″	″	″	″	″	″	″	″	″	IK	355
7.1	none	10.12	1.02	1.01	0.32	0.42	5	2	79	18	0.51	CC, VA	1630
7.2	none	″	″	″	″	″	″	″	″	″	″	CC, VA	1020
7.3	none	″	″	″	″	″	″	″	″	″	″	CC, VA	2100
8.1	0.5 g quartz	″	″	″	″	″	″	″	″	″	″	IK	269
8.2	0.5 g quartz	″	″	″	″	″	″	″	″	″	″	IK	238
8.3	0.5 g quartz	″	″	″	″	″	″	″	″	″	″	IK	246
9.1	0.1 g mica	″	″	″	″	″	″	″	″	″	″	IK	269
9.2	0.1 g mica	″	″	″	″	″	″	″	″	″	″	IK	294
9.3	0.1 g mica	″	″	″	″	″	″	″	″	″	″	IK	319
10.1	none	10.09	1.30	1.34	0.39	0.65	8	1.23	126	28	0.81	CC, VA	363
10.2	none	″	″	″	″	″	″	″	″	″	″	CC, VA	455
10.3	none	″	″	″	″	″	″	″	″	″	″	CC, VA	825
11.1	0.5 g quartz	″	″	″	″	″	″	″	″	″	″	IK	138
11.2	0.5 g quartz	″	″	″	″	″	″	″	″	″	″	IK	131
11.3	0.5 g quartz	″	″	″	″	″	″	″	″	″	″	IK	116
12.1	0.1 g mica	″	″	″	″	″	″	″	″	″	″	IK	138
12.2	0.1 g mica	″	″	″	″	″	″	″	″	″	″	IK	81
12.3	0.1 g mica	″	″	″	″	″	″	″	″	″	″	IK	75
13.1	none	10.07	1.57	1.66	0.45	0.92	11	0.92	174	40	1.1	CC, VA	429
13.2	none	″	″	″	″	″	″	″	″	″	″	CC, VA	440
13.3	none	″	″	″	″	″	″	″	″	″	″	CC, VA	570
14.1	0.5 g quartz	″	″	″	″	″	″	″	″	″	″	IK	92
14.2	0.5 g quartz	″	″	″	″	″	″	″	″	″	″	IK	55
14.3	0.5 g quartz	″	″	″	″	″	″	″	″	″	″	IK	82
14.4	5 g quartz	″	″	″	″	″	″	″	″	″	″	IK	130
14.5	10 g quartz	″	″	″	″	″	″	″	″	″	″	IK	114
15.1	0.1 g mica	″	″	″	″	″	″	″	″	″	″	IK	46
15.2	0.1 g mica	″	″	″	″	″	″	″	″	″	″	IK	82
15.3	0.1 g mica	″	″	″	″	″	″	″	″	″	″	IK	50
15.4	5 g mica	″	″	″	″	″	″	″	″	″	″	IK	51
15.5	10 g mica	″	″	″	″	″	″	″	″	″	″	IK	45
16.1	none	10.04	1.83	1.97	0.51	1.2	15	0.72	229	51	1.5	IK	43
16.2	none	″	″	″	″	″	″	″	″	″	″	IK	51
16.3	none	″	″	″	″	″	″	″	″	″	″	IK	62
17.1	0.5 g quartz	″	″	″	″	″	″	″	″	″	″	IK	94
17.2	0.5 g quartz	″	″	″	″	″	″	″	″	″	″	IK	43
17.3	0.5 g quartz	″	″	″	″	″	″	″	″	″	″	IK	43
18.1	0.1 g mica	″	″	″	″	″	″	″	″	″	″	IK	39
18.2	0.1 g mica	″	″	″	″	″	″	″	″	″	″	IK	48
18.3	0.1 g mica	″	″	″	″	″	″	″	″	″	″	IK	44
19.1	none	10.02	2.07	2.29	0.56	1.5	18	0.63	288	65	1.9	IK	N/A
19.2	none	″	″	″	″	″	″	″	″	″	″	IK	N/A
19.3	none	″	″	″	″	″	″	″	″	″	″	IK	N/A
20.1	0.5 g quartz	″	″	″	″	″	″	″	″	″	″	IK	N/A

(*continued on next page*)

Table 1 (*continued*)

Experiment		Solution speciation[a]					Saturation[a]					Precipitates and t_{ind}	
Exp no	Substrate	pH	a^{2+}_{Ca} [mM]	a^{-}_{HCO3} [mM]	a^{2-}_{CO3} [mM]	a^{0}_{CaCO3} [mM]	Ω_{ikaite}	$\log^{-2}\Omega_{ikaite}$	Ω_{CC}[b]	Ω_{VA}[b]	Ω_{ACC}[b]	Phase[b]	t_{ind} [s]
20.2	0.5 g quartz	〃	〃	〃	〃	〃	〃	〃	〃	〃	〃	IK	N/A
20.3	0.5 g quartz	〃	〃	〃	〃	〃	〃	〃	〃	〃	〃	IK	N/A
21.1	0.1 g mica	〃	〃	〃	〃	〃	〃	〃	〃	〃	〃	IK	N/A
21.2	0.1 g mica	〃	〃	〃	〃	〃	〃	〃	〃	〃	〃	IK	N/A
21.3	0.1 g mica	〃	〃	〃	〃	〃	〃	〃	〃	〃	〃	IK	N/A
22.1	none	10.00	2.31	2.60	0.61	1.81	22	0.55	347	78	2.2	IK	N/A
22.2	none	〃	〃	〃	〃	〃	〃	〃	〃	〃	〃	IK	N/A
22.3	none	〃	〃	〃	〃	〃	〃	〃	〃	〃	〃	IK	N/A
23.1	0.5 g quartz	〃	〃	〃	〃	〃	〃	〃	〃	〃	〃	IK	N/A
23.2	0.5 g quartz	〃	〃	〃	〃	〃	〃	〃	〃	〃	〃	IK	N/A
23.3	0.5 g quartz	〃	〃	〃	〃	〃	〃	〃	〃	〃	〃	IK	N/A
24.1	0.1 g mica	〃	〃	〃	〃	〃	〃	〃	〃	〃	〃	IK	N/A
24.2	0.1 g mica	〃	〃	〃	〃	〃	〃	〃	〃	〃	〃	IK	N/A
24.3	0.1 g mica	〃	〃	〃	〃	〃	〃	〃	〃	〃	〃	IK	N/A
25.1	none	9.98	2.53	2.91	0.66	2.13	26	0.50	407	91	2.6	IK	N/A
25.2	none	〃	〃	〃	〃	〃	〃	〃	〃	〃	〃	IK	N/A
25.3	none	〃	〃	〃	〃	〃	〃	〃	〃	〃	〃	IK	N/A
26.1	0.5 g quartz	〃	〃	〃	〃	〃	〃	〃	〃	〃	〃	IK	N/A
26.2	0.5 g quartz	〃	〃	〃	〃	〃	〃	〃	〃	〃	〃	IK	N/A
26.3	0.5 g quartz	〃	〃	〃	〃	〃	〃	〃	〃	〃	〃	IK	N/A
27.1	0.1 g mica	〃	〃	〃	〃	〃	〃	〃	〃	〃	〃	IK	N/A
27.2	0.1 g mica	〃	〃	〃	〃	〃	〃	〃	〃	〃	〃	IK	N/A
27.3	0.1 g mica	〃	〃	〃	〃	〃	〃	〃	〃	〃	〃	IK	N/A
28.1	none	9.90	3.77	4.70	0.87	4.20	51	0.34	794	182	5	IK	N/A
28.2	none	〃	〃	〃	〃	〃	〃	〃	〃	〃	〃	IK	N/A
28.3	none	〃	〃	〃	〃	〃	〃	〃	〃	〃	〃	IK	N/A
29.1	0.5 g quartz	〃	〃	〃	〃	〃	〃	〃	〃	〃	〃	IK	N/A
29.2	0.5 g quartz	〃	〃	〃	〃	〃	〃	〃	〃	〃	〃	IK	N/A
29.3	0.5 g quartz	〃	〃	〃	〃	〃	〃	〃	〃	〃	〃	IK	N/A

[a] Solution speciation and saturation were calculated using PHREEQC (Parkhurst and Appelo, 2013).
[b] CC: calcite, VA: vaterite, IK: ikaite, ACC: amorphous calcium carbonate.

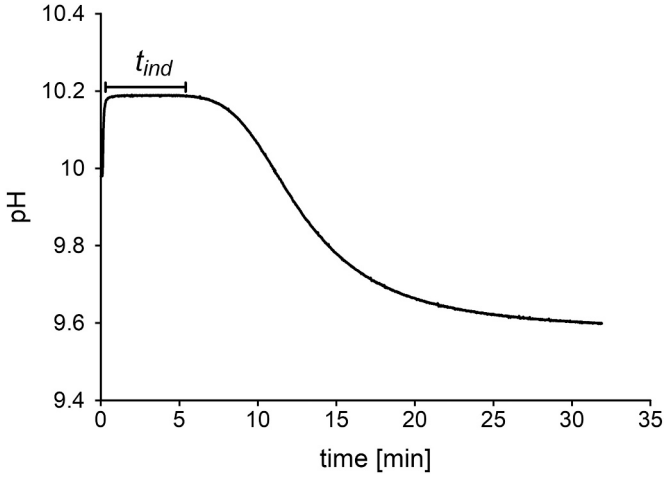

Fig. 2. pH versus time plot for an CMBR experiment with a solution of $\Omega_{ikaite} = 5$ at $T = 0$ °C. Precipitation of the carbonate phase (ikaite) caused a decrease of pH indicating the induction of precipitation t_{ind}.

in contrast, ikaite precipitated over the whole range of supersaturation $1.6 \leq \Omega_{ikaite} \leq 51$ (Fig. 3B). Experiments with increased amounts of substrates (5 g, 10 g) did neither cause a change in the phase inventory nor a significant reduction of t_{ind} (Fig. 4). In order to attain comparable conditions, the minimum amounts of crystals (0.5 g quartz, 0.1 g mica) have been added to the experiments by default.

Besides crystalline phases, an amorphous phase was found in X-ray analyses of solids from CMBR experiments with an initial supersaturation $\Omega_{ikaite} \geq 26$, if the samples were retrieved within the first 30 s of the experimental run. During repeated X-ray diffraction scans (each taken over 3 min at room temperature on a pre-cooled but warming sample holder), the amorphous phase transformed into calcite and vaterite (Figs. S4–S5). If the solids were retrieved from reactor later than 30 s after starting the experimental run, the amorphous phase was no longer detectable by X-ray analysis.

Cryo SEM revealed different morphologies of precipitates depending on the moment they were retrieved from CMBR (Fig. 5). Precipitates retrieved within the first 30 s after attaining a supersaturated solution consisted of granules partly forming larger anhedral units or aggregates with diameters up to 2 μm (Fig. 5A). Very few euhedral platelets coexist with the granular mass at this early stage of experiments (Fig. 5B). In samples which were retrieved at a later stage of experiments, however, these euhedral crystals became the sole phase while the granular shaped phase vanished (Fig. 5C, D).

3.2. Desupersaturation of solutions and solubility of precipitated phases

The evolution of pH during precipitation from supersaturated solution led to a reproducible curve shape in pH vs. time graphs (Fig. 6). The pH values were plotted from the moment of addition of the carbonate containing solution to the Ca^{2+} solution within the reactor (0 s). Upon addition, the pH value increased for a few seconds until the two solutions were homogeneously mixed within the reactor. In the subsequent period, the curve approached a constant pH until nucleation of any carbonate containing phase consumed alkaline solutes which then resulted in a decrease of solution pH. The end of the precipitation process within the reactor is marked by the two electrodes attaining constant values. These values then reflect that the composition of solution within the reactor reached the solubility of the precipitated phase.

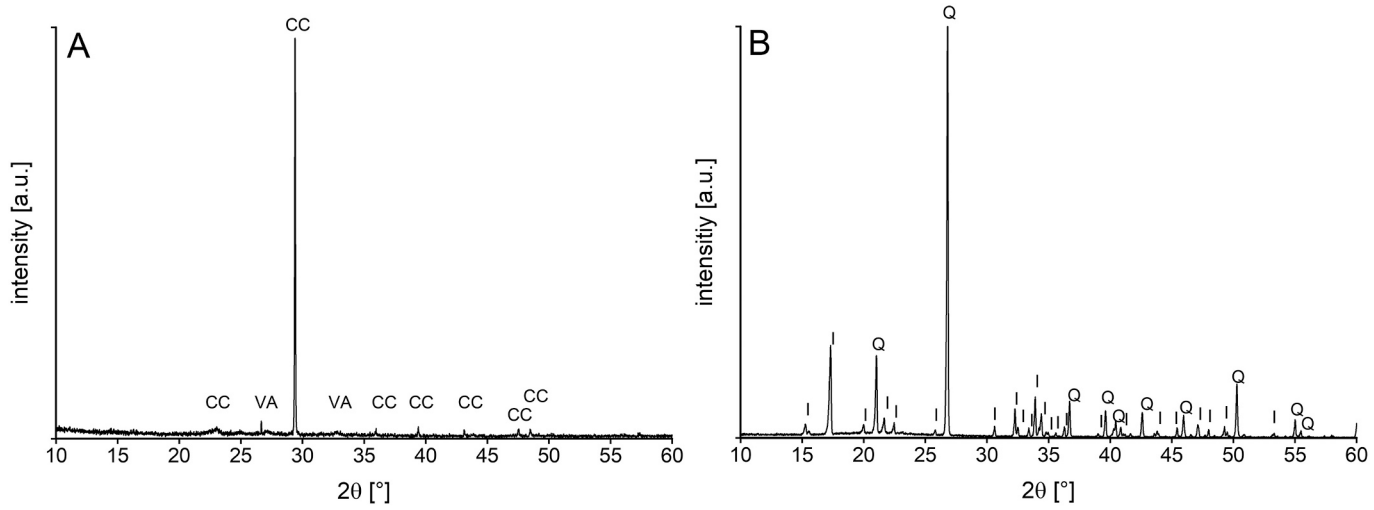

Fig. 3. X-ray diffractogram (CuKα) of precipitates retrieved from CMBR experiments. **A)** In absence of quartz or mica substrates with an initial supersaturation of $\Omega_{\text{ikaite}} = 11$ (exp. # 13.1). Diffraction peaks correspond to calcite (CC) and vaterite (VA). **B)** In presence of quartz substrates with an initial supersaturation of $\Omega_{\text{ikaite}} = 22$ (exp. # 23.3). Diffraction peaks correspond to ikaite (I) and quartz (Q).

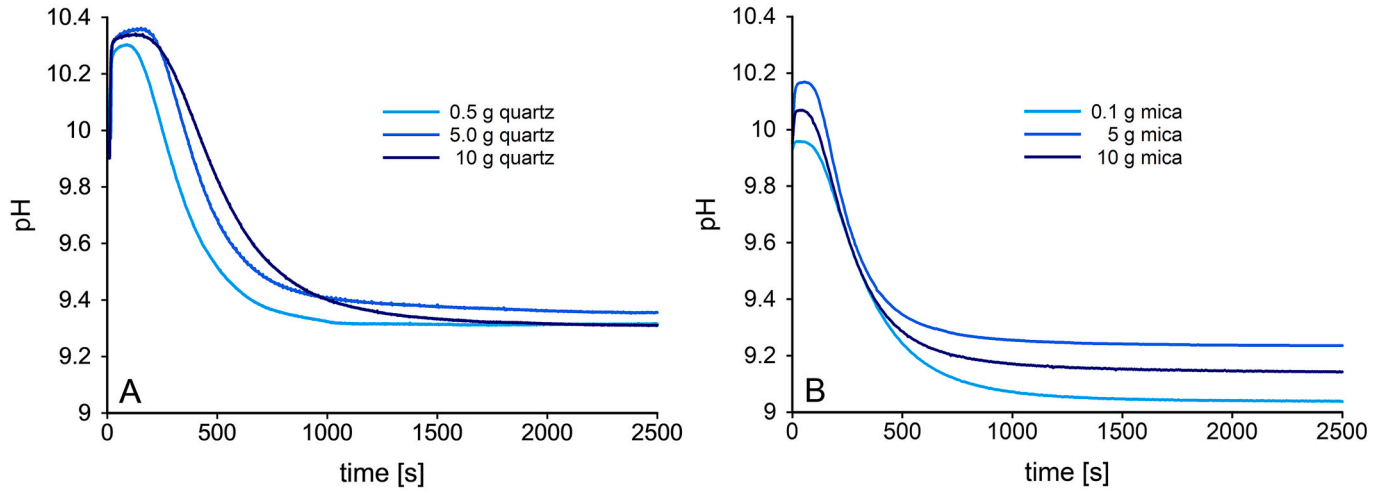

Fig. 4. Desupersaturation curves from CMBR experiments with an initial supersaturation of $\Omega_{\text{ikaite}} = 11$. **A)** In presence of different amounts of quartz. **B)** In presence of different amounts of mica.

Comparisons of solution composition are compiled in Tables S1-S3. From the data, the solubility constant for ikaite ($T = 0$ °C) can be derived:

$$log K_{sp\ \ \text{ikaite}} = -7.3 \pm 0.1$$

This value agrees well with the value $\log K_{sp\ \ \text{ikaite}} = -7.2$ reported by Bischoff et al. (1993a). The solubility constant of Bischoff et al. (1993a) is most appropriate for comparison because it was derived from experiments at temperatures down to 0.3 °C.

Desupersaturation curves originating from pseudohomogeneous precipitation matched with those recorded in presence of quartz or mica at supersaturations $\Omega_{\text{ikaite}} \geq 15$ and show the decrease of pH due to fast ikaite formation (Fig. 6B). In more diluted solutions, however, the pH evolutions in substrate-free experiments (Table 1, exp. # 1, 4, 7, 10, 13) were different compared to experiments that contain quartz or mica (Table 1, exp. # 2, 3, 5, 6, 8, 9, 11, 12, 14, 15). The pH evolution in the substrate-free runs showed a significantly extended induction time. Furthermore, pH approached a constant value which was lower compared to experiments with quartz or mica substrates. Correspondingly, precipitates retrieved from substrate equipped reactors were calcite and vaterite instead of ikaite. Noteworthy, desupersaturation curves of solutions in presence of quartz compared to mica did not show a significantly different pH evolution.

A further detail in the desupersaturation curves needs to be pointed out: In all experiments with a supersaturation $\Omega_{ikaite} \geq 18$ (irrespectively of the presence of substrates), the decrease of supersaturation caused by nucleating/growing carbonate phases was coming to a temporary halt or slow-down resulting in a kink in the shape of the desupersaturation curves (labelled with arrows in Fig. 7). The halt or slow-down typically took place ca. 1 min after the start of desupersaturation and lasted for less than a minute until eventually desupersaturation continued. The phenomenon was clearly detectable in both the pH-value and the Ca^{2+} concentration resulting from the potential of the Ca^{2+}-ISE (Fig. 7).

3.3. Induction periods of ikaite formation (t_{ind}) and interfacial energy γ

In our study, induction periods for ikaite formation were obtained from desupersaturation curves in experiments covering the range $1.6 \leq \Omega_{\text{ikaite}} \leq 15$. At supersaturations $\Omega_{\text{ikaite}} \geq 18$, the occurrence of an amorphous phase along with the kinky shape of the desupersaturation curves disabled determination of t_{ind} for ikaite. Table 1 shows the results of all t_{ind} values for ikaite precipitation as a function of solution

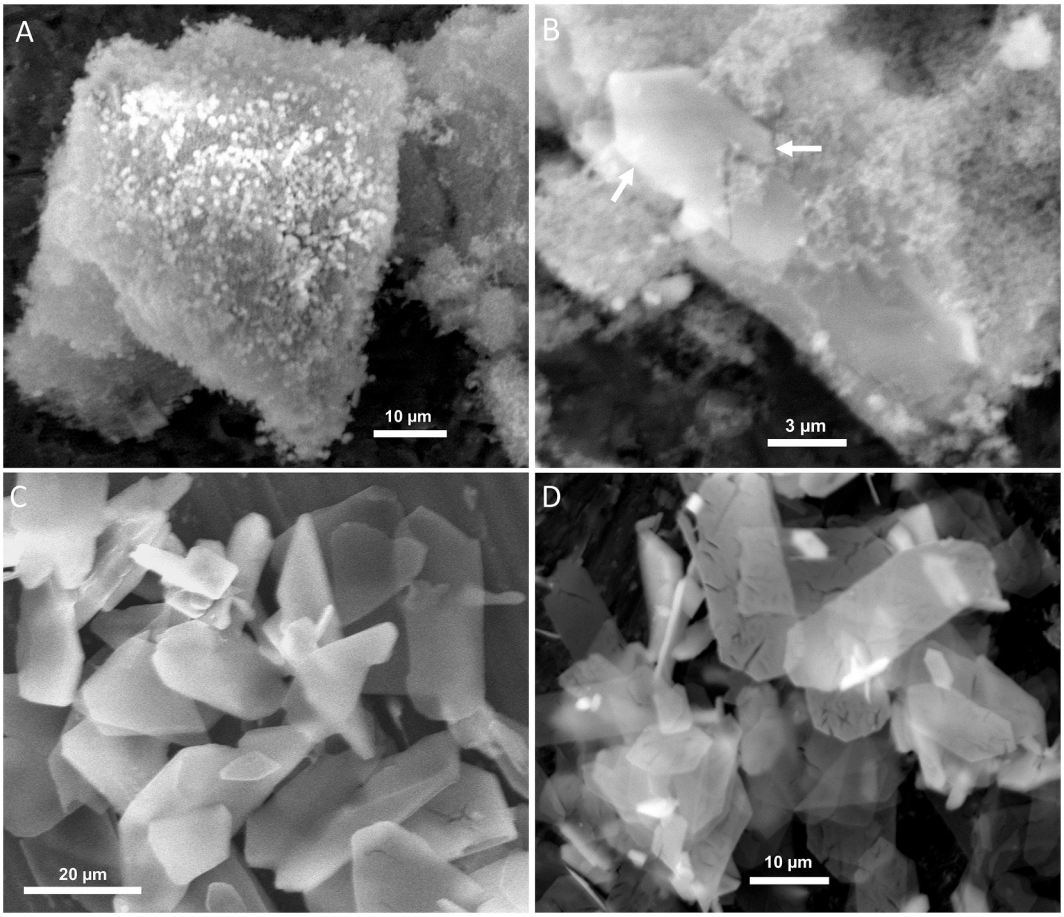

Fig. 5. Cryo SEM images of precipitates retrieved from CMBR experiments ($\Omega_{ikaite} = 51$) at different moments of desupersaturation. **A, B)** In samples retrieved within 30 s of attaining supersaturation, granular shaped fine precipitates forming larger aggregates and very few euhedral platelet-shaped crystals (white arrows in image B) were detected. **C)** Samples retrieved between 30 and 60 s of attaining supersaturation show euhedral platelet-shaped crystals exclusively. **D)** Samples retrieved after ~ 800 s of attaining supersaturation did not show any further changes in the phase inventory.

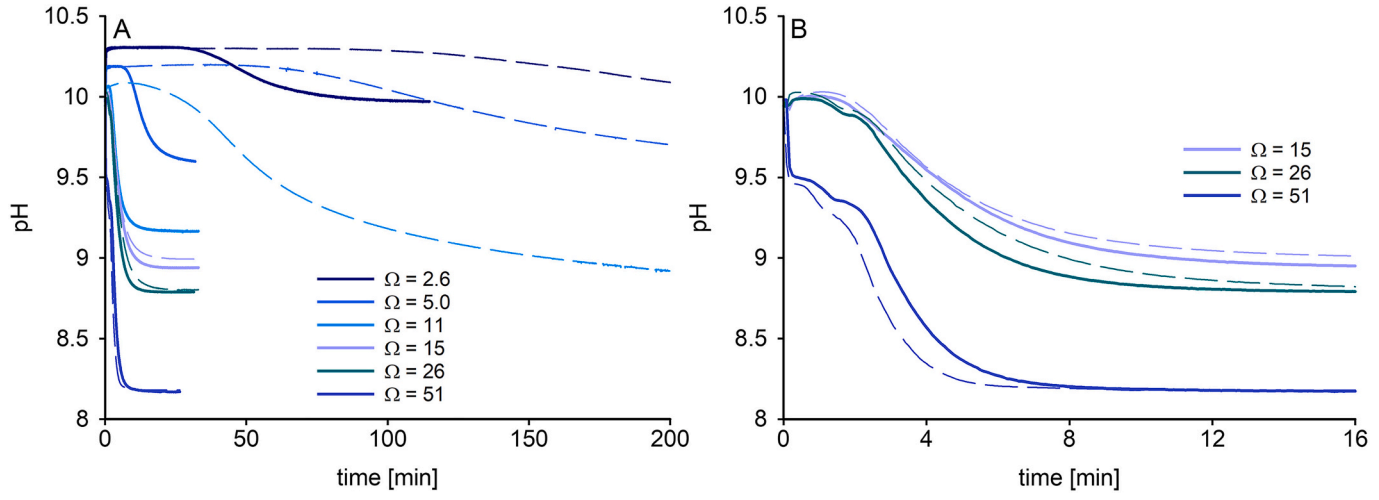

Fig. 6. A) Desupersaturation curves from CMBR experiments in presence of quartz substrates (solid lines) and at pseudohomogeneous conditions (dotted lines). **B)** Zoom into desupersaturation curves of (A). The curves shown are from experiments with supersaturations with respect to ikaite $\Omega_{ikaite} = 15$, 26, and 51.

conditions in absence and presence of quartz or mica.

Induction periods of ikaite formation t_{ind} were plotted versus the reciprocal square of the logarithm of the supersaturation with respect to ikaite $(\log \Omega)^{-2}$ (Fig. 8). As shown in Fig. 8A, separate linear regressions within two different supersaturation ranges (above and below $\log^{-2} \Omega = 1.23$) provide good fits to our data. The interfacial energy γ between a spherical ikaite nuclei ($\beta = 16\pi/3$) and solution was calculated using the slope B from data at $\log^{-2} \Omega \leq 1.23$. In this range of supersaturations, t_{ind} was not significantly affected by the presence or absence of quartz or mica. Both types of experiments yielded slopes of $0.68 \leq B \leq 0.73$ (Fig. 8B). A value of 15 mJ/m^2

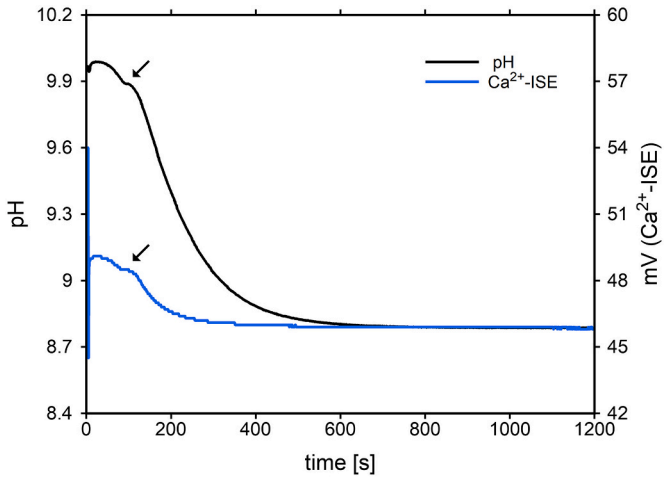

Fig. 7. Desupersaturation curves (pH and Ca^{2+}-ISE-potential) from an CMBR experiment with an initial degree of supersaturation $\Omega_{ikaite} = 26$. After an initial decrease of pH and mV, the signals remained constant for a few seconds (arrows) until desupersaturation continued.

(± 3 mJ/m^2) resulted for the effective interfacial energy by using all experimental data (with and without substrates).

The regression of t_{ind} at $\log^{-2} \Omega > 1.23$ indicates a decreased interfacial energy. Application of Eq. (6) yielded a value of 6 mJ/m^2 (±3 mJ/m^2) for the interfacial energy from the regression of the combined quartz and mica data. It needs to be noted, however, that $f(\theta) = 1$ in Eq. (6) is only valid for homogeneous nucleation. In the case of heterogeneous nucleation, a decreased value for $f(\theta)$ leads to an increased value for the interfacial energy. At present, however, it remains unclear by how much $f(\theta)$ is reduced.

Besides interfacial energies of ikaite, those of calcite and vaterite were calculated using induction periods from CMBR experiments which led to the formation of anhydrous calcium carbonates ($\Omega_{ikaite} \leq 11$). These calculations are both based on 15 induction periods which were determined for five different supersaturations in absence of mineral substrates (Table 1, exp. # 1, 4, 7, 10, 13) (Fig. 9). By using the same experimental t_{ind} values for both phases, inserting individual values for the molar volume of calcite and vaterite, respectively, and taking into account the respective supersaturations, Eq. (6) yielded a value of 58 mJ/m^2 (± 3 mJ/m^2) for $\gamma_{calcite}$ and 35 mJ/m^2 (± 3 mJ/m^2) for $\gamma_{vaterite}$.

4. Discussion

4.1. Formation conditions of ikaite

In substrate-free experiments with a supersaturation $\Omega_{ikaite} \leq 11$ (pH ≈ 10.0), no ikaite but calcite and vaterite precipitated at $T = 0$ °C. Ikaite precipitation was observed in substrate-free solutions with higher supersaturations instead. This finding agrees well with previously reported inhibitor-free formation conditions of ikaite in alkaline solutions (pH > 11) (Boch et al., 2015; Hu et al., 2015; Rodríguez-Ruiz et al., 2014).

Quartz or mica added to the reactor led to ikaite nucleation over a much broader supersaturation range than in substrate free experiments. Even in solutions with a supersaturation of $\Omega_{ikaite} = 1.6$, promotion of ikaite formation by quartz or mica surpassed any possible promotion of the formation of anhydrous phases. Similarly strong effects leading to the nucleation of ikaite rather than anhydrous calcium carbonate

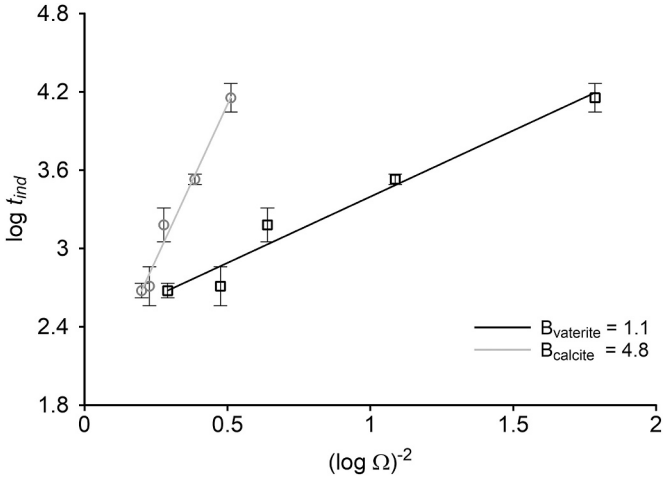

Fig. 9. Plot of log t_{ind} vs. $(\log \Omega)^{-2}$ for calcite/vaterite formation in absence of mineral substrates.

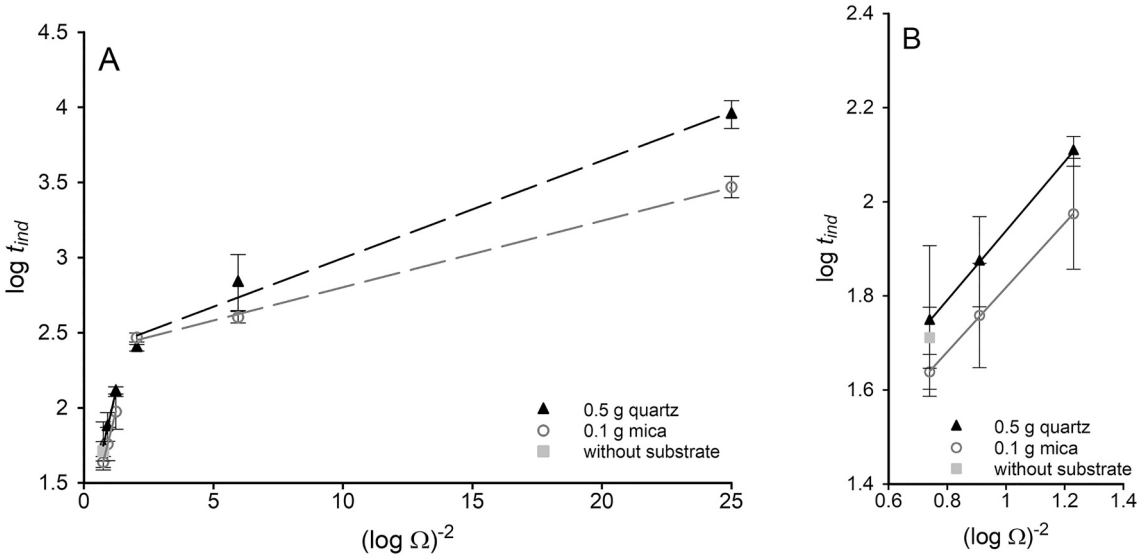

Fig. 8. Plot of log t_{ind} vs. $(\log \Omega)^{-2}$ for ikaite formation in absence (grey squares) and presence of quartz (black triangles) and mica (open circles) substrates, respectively. **A)** Two dashed lines represent linear regressions of the data obtained in experiments with $\log^{-2} \Omega_{ikaite} > 1.23$ ($B_{mica} = 0.04$ and $B_{quartz} = 0.06$). **B)** Enlarged illustration of the data obtained at $\log^{-2} \Omega_{ikaite} \leq 1.23$. The lines represent linear regressions of the respective data points.

minerals were previously attributed to calcite-inhibiting additives like Mg^{2+} and phosphate exclusively (e.g., Hu et al., 2015; Stockmann et al., 2018; Tollefsen et al., 2018). Our results, though, show that the presence of mineral surfaces in general play an important role for ikaite formation. A comprehensive understanding of the ikaite formation conditions in natural settings, therefore, requires consideration not only of the presence of calcite-inhibiting substances but also of the presence or absence of mineral surfaces capable of promoting heterogeneous nucleation of ikaite.

4.2. The occurrence of an amorphous phase at elevated Ω_{ikaite}

At elevated supersaturations ($\Omega_{ikaite} \geq 15$), ikaite formation was largely unaffected by the presence or absence of quartz or mica substrates. According to the classical nucleation theory (Kashchiev and van Rosmalen, 2003; Mullin, 2001; Sangwal, 2007), such a behaviour is not uncommon and may be explained with (pseudo-)homogeneous or volume nucleation in which the rate of nucleation within the bulk solution is so fast that substrate induced nuclei do not any longer contribute to the overall nucleation rate significantly. In this type of experiments, desupersaturation of the solution caused by ikaite nucleation and growth was characterized by a continuous decrease of pH-value and Ca^{2+}-concentration (i.e., potential of Ca^{2+}-ISE). However, the range of experimental starting conditions, which led to such a continuous decrease of pH and Ca^{2+}-concentration, was narrow. In experiments starting at supersaturations $\Omega_{ikaite} \geq 18$, desupersaturation curves revealed a kinky shape by a temporary halt or slow-down of proton release and Ca^{2+}-consumption (Fig. 6). This implies a transient stop or retardation of total calcium carbonate precipitation within the reactor and, therefore, a modified mechanism of carbonate precipitation within the reactor. In fact, the phases detected in the precipitates of these experiments depended on the time when the precipitate was retrieved from the reactor. In experiments running for >30 s, ikaite was detected (as in the case of experiments started at $\Omega_{ikaite} < 18$). X-ray analyses of precipitates retrieved from the reactor within the first 30 s after mixing, however, did not reveal ikaite (Table 1, exp. # 19–29). At this early stage of experiments, though, the total amount of precipitate often was too low for successful X-ray analyses. Only experiments with an initial supersaturation of at least $\Omega_{ikaite} \geq 26$ provided the necessary sample mass to detect an amorphous phase. Cryo-SEM provided more detailed information about the phase inventory of precipitates from this early stage of CMBR experiments ($\Omega_{ikaite} = 51$). The SEM-images revealed significant amounts of amorphous phase besides very few ikaite crystals. As all experiments in the supersaturation range $18 \leq \Omega_{ikaite} \leq 51$ show comparable kink shapes in the pH and Ca^{2+}-concentration curves, an initial presence of an amorphous phase must be inferred at least for this entire saturation range.

A similar evolution of desupersaturation curves for the precipitation of ikaite from alkaline solutions at elevated Ω_{ikaite} was reported by Zou et al. (2018). These authors state that an amorphous calcium carbonate phase was formed instantaneously while pH and potential of Ca^{2+}-ISE reached a constant value before a subsequent decrease of both pH and Ca^{2+}-concentration indicated rapid nucleation and growth of ikaite. Our findings are further corroborated by Besselink et al. (2017) who observed the formation of an amorphous calcium carbonate precursor which likely started disappearing during the crystallization of ikaite in a highly supersaturated solution at low temperatures (2–12 °C). Despite these observations at conditions different to ours, evidence for the ikaite formation mechanism in the presence of an amorphous phase valid over the entire range of conditions is missing still. At least at the conditions applied here, the coexistence of the amorphous phase and ikaite shown in cryo SEM images (Fig. 5B) implies that ikaite nucleates independently of the amorphous phase.

4.3. Interfacial energy and the effect of substrates

The effect of quartz and mica on the formation of ikaite was pronounced at supersaturations $\Omega_{ikaite} < 15$ as these minerals controlled the nucleating phase. In classical nucleation theory (CNT), this control is attributed to the interfacial energy which is reduced by foreign surfaces leading to a lower nucleation barrier. Therefore, interfacial energy is an essential quantity revealing the effect of foreign surfaces on nucleation. Our data were permissive of estimating the effective interfacial energy of ikaite from experimentally determined induction periods t_{ind} by applying CNT. In general, CNT had been used to discuss the various complex pathways of calcium carbonate nucleation (e.g., De Yoreo et al., 2013; Gómez-Morales et al., 1996; Hamm et al., 2014; Hu et al., 2012; Li et al., 2014; Lioliou et al., 2007; Söhnel and Mullin, 1978). Judging by these studies, CNT may provide a useful approach to an interpretation of nucleation kinetics, even if nucleation pathways are diverse and do not completely agree with a classical description of nucleation (van Driessche et al., 2019).

According to CNT, a linear relationship between log t_{ind} and $\log^{-2}\Omega_{ikaite}$ marks a range of experimental conditions, in which the interfacial energy of ikaite and, therefore, the nucleation mechanism is supposed to be constant. Experimental log t_{ind} vs. $\log^{-2}\Omega$ data often reveal two different linear ranges (e.g., He et al., 1994; Lancia et al., 1999; Söhnel and Mullin, 1978): at low values of $\log^{-2}\Omega$ with a high interfacial energy and vice versa. The high energy relates to homogeneous nucleation whereas the low energy points towards heterogeneous nucleation. The log t_{ind} vs. $\log^{-2}\Omega_{ikaite}$ data derived from our experiments obviously also reveal two ranges with linear relationships (Fig. 8A): *i)* $\Omega_{ikaite} \geq 8$ ($\log^{-2}\Omega_{ikaite} \leq 1.23$) and *ii)* $\Omega_{ikaite} \leq 5$ ($\log^{-2}\Omega_{ikaite} \geq 2$).

In the higher supersaturation range (*i*), an effective interfacial energy of 15 mJ/m^2 (± 3 mJ/m^2) was obtained by assuming homogeneously formed nuclei (i.e., correction factor $f(\theta) = 1$) with a spherical shape (i.e., shape factor $\beta = 16\pi/3$) (Mullin, 2001; Söhnel and Mullin, 1988). In the low range of supersaturation (*ii*), ikaite was only forming, if minerals were present in the reactor. A value of 6 mJ/m^2 (± 3 mJ/m^2) resulted for the interfacial energy in this range. For the calculation, the same shape and correction factors as above were used. This low interfacial energy supports the assumption that heterogeneous nucleation dominated range (*ii*). As mentioned above, however, a lower correction factor (e.g., Söhnel and Handlířová, 1984) may lead to a higher interfacial energy. This may limit the applicability of Eqns. (4)–(6) for the interpretation of our data. Also, the transition between the two linear ranges of log t_{ind} vs. $\log^{-2}\Omega$ data located between $5 \leq \Omega_{ikaite} \leq 8$ does not precisely coincide with our observation that ikaite nucleates from solutions with $\Omega_{ikaite} < 15$ solely in presence of quartz or mica. At this point, applicability of CNT interpreting our experimental data obviously reaches its limitation.

Our result of 15 mJ/m^2 (± 3 mJ/m^2) for γ_{ikaite} is remarkably low compared to reported interfacial energies between nuclei of anhydrous calcium carbonates and solution. Söhnel and Mullin (1978) determined a theoretical value of $\gamma_{CaCO_3} = 124$ mJ/m^2 and an experimental value of 83 mJ/m^2. Lower values of interfacial energies of calcite (e.g.,$\gamma = 64$ mJ/m^2, Lioliou et al., 2007) and vaterite (e.g., $\gamma = 37$ mJ/m^2, Verdoes et al., 1992; $\gamma = 41$ mJ/m^2, Gómez-Morales et al., 1996) have also been reported and were attributed to some degree of heterogeneous nucleation. The latter interfacial energies well agree with our values of $\gamma_{vaterite} = 35$ mJ/m^2 (± 3 mJ/m^2) and $\gamma_{calcite} = 58$ mJ/m^2 (± 3 mJ/m^2) for pseudohomogeneous nucleation. Li et al. (2014) reported interfacial energies with values between 47 and 24 mJ/m^2 for vaterite and calcite nuclei on quartz and mica substrates. The results of Li et al. (2014) imply that quartz and mica substrates may contribute to the formation of anhydrous $CaCO_3$ phases by decreasing the interfacial energy of nuclei.

Two points should be noted here. Firstly, our values for γ_{ikaite} (irrespectively of the presence or absence of mineral substrates) are significantly lower compared to the values of anhydrous $CaCO_3$ phases. This clearly reflects the highly hydrated character of the ikaite structure involving predominantly weak hydrogen bonds at the interface.

Secondly, the value of interfacial energy within the lower supersaturation range is not reduced by much (from 15 to 6 mJ/m^2). This may indicate that the contribution of the ikaite-substrate interface to the reduction of the nucleation barrier is less compared to the contribution of interfaces between anhydrous calcium carbonates and substrates. This low interfacial contribution to ikaite formation might as well be associated with its highly hydrated character and might reflect the low energy formation pathway of ikaite nucleation as suggested by Chaka (2018) via an assemblage of aqueous $CaCO_3^0x6H_2O$ complexes. Substrates, in this case, would promote an accumulation of the hydrous pair complexes rather than a dehydration of aqueous ionic complexes – as it is the case for nucleation of anhydrous phases. The similar degree of promotion of ikaite nucleation by mica and quartz might indicate that the similar surface chemical characteristics of these two minerals affect heterogeneous nucleation much stronger than their different surface structural characteristics. This finding contrasts with the effects of quartz and mica on anhydrous $CaCO_3$ nuclei which were assumed being dependent on the degree of lattice fit (Li et al., 2014). In the range of conditions examined here, one might speculate that the velocity of structural ordering of adsorbed complexes at the interface is not the rate determining step for heterogeneous ikaite nucleation. At $\Omega_{ikaite} = 1.6$, the similarity of the promotion by mica and quartz weakens. The experimental approach of this study, however, is inapt to test whether the dissimilarity becomes significant at $\Omega_{ikaite} < 1.6$. At such low supersaturations, the induction periods rise to many hours or even days. Within these long periods, artefacts due to unavoidable impurities within the reactor cannot be excluded any longer.

From our results it can be suggested that the phase formation kinetics at cold temperatures is controlled by the condition whether solutes are required to dehydrate or not. Because the formation rate of the amorphous phase in our experiments is at least as fast as the ikaite formation rate, it must be hypothesized that the amorphous phase is highly hydrated as well. Such a highly hydrated phase would agree with an extensive polyamorphism of calcium carbonate which involves varying water contents (Cartwright et al., 2012). The formation rate of a lowly hydrated phase may not compete with the formation rate of ikaite at temperatures close to the freezing point of water. A lowly hydrated amorphous phase, though, might form via a dehydration of $CaCO_3x6H_2O$ phases (Addadi et al., 2003; Tlili et al., 2002). Subsequently, such a lowly hydrated phase may lead to anhydrous calcium carbonates (Besselink et al., 2017; Radha et al., 2010).

5. Conclusions

The presence of quartz or mica surfaces led to nucleation of ikaite over a significantly broader supersaturation range than at substrate free conditions. A pronounced promotion of ikaite nucleation by quartz and mica, which exceeded a potential promotion of anhydrous calcium carbonates, was observed at supersaturations Ω_{ikaite} ranging from 1.6 to 15. For the (pseudo-) homogeneous nucleation of ikaite, the application of CNT on induction periods t_{ind} yielded an effective interfacial energy of 15 mJ/m^2 ($\pm$3 mJ/m^2), which is significantly lower than reported values for anhydrous calcium carbonates. This low interfacial energy supports the idea of a low energy formation pathway of ikaite that involves a dominant role of aqueous ion pair complexes. At more elevated supersaturations ($\Omega_{\mathrm{ikaite}} \geq 18$), a transient amorphous phase forms parallel to ikaite.

Declaration of Competing Interest

The authors declare that they have no known competing financial interests or personal relationships that could have appeared to influence the work reported in this paper.

Data availability

No data was used for the research described in the article.

Acknowledgements

The authors thank Giuseppe Saldi for his kind assistance with BET measurements, Stefanie Janke & Moritz Zenkert for lab assistance, and Andreas Götz (Ziegler Minerals, Wunsiedel, Germany) for providing excellent mica minerals. Furthermore, the authors are grateful for two anonymous reviews and the editorial handling by Michael E. Böttcher. Financial support of this study by the Deutsche Forschungsgemeinschaft DFG (JO301/6-1) is gratefully acknowledged.

Appendix A. Supplementary data

Supplementary data to this article can be found online at https://doi.org/10.1016/j.chemgeo.2022.121089.

References

Addadi, L., Raz, S., Weiner, S., 2003. Taking advantage of disorder: amorphous calcium carbonate and its roles in biomineralization. Adv. Mater. 15 (12), 959–970. https://doi.org/10.1002/adma.200300381.

Besselink, R., Rodriguez-Blanco, J.D., Stawski, T.M., Benning, L.G., Tobler, D.J., 2017. How short-lived ikaite affects calcite crystallization. Cryst. Growth Des. 17 (12), 6224–6230.

Bischoff, J.L., Fitzpatrick, J.A., Rosenbauer, R.J., 1993a. The solubility and stabilization of Ikaite (CaCO3· 6H2O) from 0° to 25°C: environmental and paleoclimatic implications for Thinolite Tufa. J. Geol. 101 (1), 21–33.

Bischoff, J.L., Rosenbauer, R.J., Fitzpatrick, J.A., Stafford Jr., T.W., 1993b. Ikaite precipitation by mixing of shoreline springs and Lake water, Mono Lake, California, USA. Geochimica et Cosmochimica 57 (16), 3855–3865.

Blue, C.R., Giuffre, A., Mergelsberg, S., Han, N., de Yoreo, J.J., Dove, P.M., 2017. Chemical and physical controls on the transformation of amorphous calcium carbonate into crystalline CaCO3 polymorphs. Geochim. Cosmochim. Acta 196, 179–196. https://doi.org/10.1016/j.gca.2016.09.004.

Boch, R., Dietzel, M., Reichl, P., Leis, A., Baldermann, A., Mittermayr, F., Pölt, P., 2015. Rapid ikaite (CaCO3·6H2O) crystallization in a man-made river bed: Hydrogeochemical monitoring of a rarely documented mineral formation. Appl. Geochem. 63, 366–379.

Brečević, L., Nielsen, A.E., 1989. Solubility of amorphous calcium carbonate. J. Cryst. Growth 98 (3), 504–510.

Buchardt, B., Israelson, C., Seaman, P., Stockmann, G., 2001. Ikaite tufa towers in Ikka Fjord, Southwest Greenland: their formation by mixing of seawater and alkaline spring water. J. Sediment. Res. 71 (1), 176–189.

Cartwright, J.H.E., Checa, A.G., Gale, J.D., Gebauer, D., Sainz-Díaz, C.I., 2012. Calcium carbonate polyamorphism and its role in biomineralization: how many amorphous calcium carbonates are there? Angew. Chem. 51 (48), 11960–11970. https://doi.org/10.1002/anie.201203125 (International ed. in English).

Chaka, A.M., 2018. Ab Initio thermodynamics of hydrated calcium carbonates and calcium analogues of magnesium carbonates: implications for carbonate crystallization pathways. ACS Earth Space Chem. 2 (3), 210–224.

Council, T.C., Bennett, P.C., 1993. Geochemistry of ikaite formation at Mono Lake, California: implications for the origin of tufa mounds. Geology 21 (11), 971–974.

De Yoreo, J.J., Waychunas, G.A., Jun, Y.-S., Fernandez-Martinez, A., 2013. In situ investigations of carbonate nucleation on mineral and organic surfaces. Rev. Mineral. Geochem. 77 (1), 229–257. https://doi.org/10.2138/rmg.2013.77.7.

Demichelis, R., Raiteri, P., Gale, J.D., 2014. Structure of hydrated calcium carbonates: a first-principles study. J. Cryst. Growth 401, 33–37. https://doi.org/10.1016/j.jcrysgro.2013.10.064.

Dickens, B., Brown, E.W., 1970. Crystal structure of calcium carbonate hexahydrate at about −120.Deg. Inorg. Chem. 9 (3), 480–486.

Dieckmann, G.S., Nehrke, G., Papadimitriou, S., Göttlicher, J., Steininger, R., Kennedy, H., Wolf-Gladrow, D., Thomas, D.N., 2008. Calcium carbonate as ikaite crystals in Antarctic Sea ice. Geophys. Res. Lett. 35 (8).

Dieckmann, G.S., Nehrke, G., Uhlig, C., Göttlicher, J., Gerland, S., Granskog, M.A., Thomas, D.N., 2010. Brief communication: Ikaite (CaCO 3 ·6H 2 O) discovered in Arctic Sea ice. Cryosphere 4 (2), 227–230.

van Driessche, A., Stawski, T.M., Kellermeier, M., 2019. Calcium sulfate precipitation pathways in natural and engineered environments. Chem. Geol. 530, 119274 https://doi.org/10.1016/j.chemgeo.2019.119274.

Fischer, M., Thomas, D.N., Krell, A., Nehrke, G., Göttlicher, J., Norman, L., Meiners, K. M., Riaux-Gobin, C., Dieckmann, G.S., 2013. Quantification of ikaite in Antarctic Sea ice. Antarct. Sci. 25 (3), 421–432.

Gebauer, D., Cölfen, H., 2011. Prenucleation clusters and non-classical nucleation. Nano Today 6 (6), 564–584.

Gebauer, D., Kellermeier, M., Gale, J.D., Bergström, L., Cölfen, H., 2014. Pre-nucleation clusters as solute precursors in crystallisation. Chem. Soc. Rev. 43 (7), 2348–2371. https://doi.org/10.1039/c3cs60451a.

Geilfus, N.-X., Carnat, G., Dieckmann, G.S., Halden, N., Nehrke, G., Papakyriakou, T., Tison, J.-L., Delille, B., 2013. First estimates of the contribution of CaCO 3 precipitation to the release of CO 2 to the atmosphere during young sea ice growth. J. Geophys. Res. Oceans 118 (1), 244–255.
Gómez-Morales, J., Torrent-Burgués, J., Rodríguez-Clemente, R., 1996. Nucleation of calcium carbonate at different initial pH conditions. J. Cryst. Growth 169 (2), 331–338.
Hamm, L.M., Giuffre, A.J., Han, N., Tao, J., Wang, D., de Yoreo, J.J., Dove, P.M., 2014. Reconciling disparate views of template-directed nucleation through measurement of calcite nucleation kinetics and binding energies. Proc. Natl. Acad. Sci. U. S. A. 111 (4), 1304–1309.
He, S., Oddo, J.E., Tomson, M.B., 1994. The nucleation kinetics of calcium sulfate dihydrate in NaCl solutions up to 6 m and 90 °C. J. Colloid Interface Sci. 162 (2), 297–303.
Hesse, K.F., Küppers, H., Suess, E., 1983. Refinement of the structure of Ikaite, CaCO3·6H2O. Zeitschrift für Kristallographie-Crystalline Materials 163 (3–4), 227–231.
Hu, Q., Nielsen, M.H., Freeman, C.L., Hamm, L.M., Tao, J., Lee, J.R.I., Han, T.Y.J., Becker, U., Harding, J.H., Dove, P.M., de Yoreo, J.J., 2012. The thermodynamics of calcite nucleation at organic interfaces: classical vs. non-classical pathways. Faraday Discuss. 159, 509.
Hu, Y.-B., Dieckmann, G.S., Wolf-Gladrow, D.A., Nehrke, G., 2014. Laboratory study on coprecipitation of phosphate with ikaite in sea ice. J. Geophys. Res. Oceans 119 (10), 7007–7015.
Hu, Y.-B., Wolthers, M., Wolf-Gladrow, D.A., Nehrke, G., 2015. Effect of pH and phosphate on calcium carbonate polymorphs precipitated at near-freezing temperature. Cryst. Growth Des. 15 (4), 1596–1601.
Ito, T., 1996. Ikaite fraom cold spring water at Shiowakka, Hokkaido, Japan. J. Mm. Petr. Econ. Geol. 91, 209–219.
Jansen, J.H.F., Woensdregt, C.F., Kooistra, M.J., van der Gaast, S.J., 1987. Ikaite pseudomorphs in the Zaire deep sea fan: an intermediate between calcite and porous calcite. Geology 15 (3), 245–248.
Johnston, J., Merwin, H.E., Williams, E.D., 1916. The several forms of calcium carbonate. Am. J. Sci. 246, 473–512.
Kashchiev, D., van Rosmalen, G.M., 2003. Review: nucleation in solutions revisited. Cryst. Res. Technol. 38 (7–8), 555–574. https://doi.org/10.1002/crat.200310070.
Lancia, A., Musmarra, D., Prisciandaro, M., 1999. Measuring induction period for calcium sulfate dihydrate precipitation. AICHE J. 45 (2), 390–397.
Li, Q., Fernandez-Martinez, A., Lee, B., Waychunas, G.A., Jun, Y.-S., 2014. Interfacial energies for heterogeneous nucleation of calcium carbonate on mica and quartz. Environ. Sci. Technol. 48 (10), 5745–5753.
Lioliou, M.G., Paraskeva, C.A., Koutsoukos, P.G., Payatakes, A.C., 2007. Heterogeneous nucleation and growth of calcium carbonate on calcite and quartz. J. Colloid Interface Sci. 308 (2), 421–428. https://doi.org/10.1016/j.jcis.2006.12.045.
Lu, Z., Rickaby, R.E., Kennedy, H., Kennedy, P., Pancost, R.D., Shaw, S., Lennie, A., Wellner, J., Anderson, J.B., 2012. An ikaite record of late Holocene climate at the Antarctic Peninsula. Earth Planet. Sci. Lett. 325-326, 108–115.
Malkaj, P., Chrissanthopoulos, A., Dalas, E., 2002. The overgrowth of calcium carbonate hexahydrate on new functionalized polymers. J. Cryst. Growth 242 (1–2), 233–238.
Marland, G., 1975. The stability of of CaCO3•6H2O (ikaite). Geochim. Cosmochim. Acta 39 (1), 83–91.
Martin, J.B., 2017. Carbonate minerals in the global carbon cycle. Chem. Geol. 449, 58–72.
Millero, F.J., 2007. The marine inorganic carbon cycle. Chem. Rev. 107 (2), 308–341. https://doi.org/10.1021/cr0503557.
Mullin, J.W., 2001. Crystallization, 4th ed. Butterworth-Heinemann, Oxford, p. 612.
Oehlerich, M., Mayr, C., Griesshaber, E., Lücke, A., Oeckler, O.M., Ohlendorf, C., Schmahl, W.W., Zolitschka, B., 2013. Ikaite precipitation in a lacustrine environment – implications for palaeoclimatic studies using carbonates from Laguna Potrok Aike (Patagonia, Argentina). Quat. Sci. Rev. 71, 46–53.
Omelon, C.R., Pollard, W.H., Marion, G.M., 2001. Seasonal formation of ikaite (CaCO3·6H2O) in saline spring discharge at Expedition Fiord, Canadian High Arctic: assessing conditional constraints for natural crystal growth. Geochimica et Cosmochimica 65 (9), 1429–1437.
Parkhurst, D.L., Appelo, C.A.J., 2013. Description of Input for PHREEQC Version 3—A Computer Program for Speciation, Batch-Reaction, One-Dimensional Transport, and Inverse Geochemical Calculations. U.S, Geological Survey, Denver, Colorado, p. 519.
Pauly, H., 1963. "IKAITE" a new mineral from Greenland. Arctic 16 (4), 263–264.
Plummer, L.N., Busenberg, E., 1982. The solubilities of calcite, aragonite and vaterite in CO2-H20 solutions between 0 and 90 °C, and an evaluation of the aqueous model for the system CaCO3-CO2-H20. Geochim. Cosmochim. Acta 6 (46), 1011–1040.
Purgstaller, B., Dietzel, M., Baldermann, A., Mavromatis, V., 2017. Control of temperature and aqueous Mg 2+ /ca 2+ ratio on the (trans-)formation of ikaite. Geochim. Cosmochim. Acta 217, 128–143.
Radha, A.V., Forbes, T.Z., Killian, C.E., Gilbert, P.U.P.A., Navrotsky, A., 2010. Transformation and crystallization energetics of synthetic and biogenic amorphous calcium carbonate. Proc. Natl. Acad. Sci. U. S. A. 107 (38), 16438–16443. https://doi.org/10.1073/pnas.1009959107.
Ridgwell, A., Zeebe, R.E., 2005. The role of the global carbonate cycle in the regulation and evolution of the Earth system. Earth Planet. Sci. Lett. 234 (3–4), 299–315. https://doi.org/10.1016/j.epsl.2005.03.006.
Rodriguez-Blanco, J.D., Shaw, S., Benning, L.G., 2011. The kinetics and mechanisms of amorphous calcium carbonate (ACC) crystallization to calcite, via vaterite. Nanoscale 3 (1), 265–271. https://doi.org/10.1039/c0nr00589d.
Rodríguez-Ruiz, I., Veesler, S., Gómez-Morales, J., Delgado-López, J.M., Grauby, O., Hammadi, Z., Candoni, N., García-Ruiz, J.M., 2014. Transient calcium carbonate hexahydrate (Ikaite) nucleated and stabilized in confined nano- and picovolumes. Cryst. Growth Des. 14 (2), 792–802.
Sánchez-Pastor, N., Oehlerich, M., Astilleros, J.M., Kaliwoda, M., Mayr, C.C., Fernández-Díaz, L., Schmahl, W.W., 2016. Crystallization of ikaite and its pseudomorphic transformation into calcite: Raman spectroscopy evidence. Geochim. Cosmochim. Acta 175, 271–281.
Sangwal, K., 2007. Additives and Crystallization Processes: From Fundamentals to Applications. Wiley, Chichester, xvi, p. 451.
Shearman, D.J., Smith, A.J., 1985. Ikaite, the parent mineral of jarrowite-type pseudomorphs. Proc. Geol. Assoc. 96 (4), 305–314.
Söhnel, O., Handlířová, M., 1984. Precipitation of strontium sulphate. Cryst. Res. Technol. 19 (4), 477–490.
Söhnel, O., Mullin, J.W., 1978. A method for the determination of precipitation induction periods. J. Cryst. Growth 44 (4), 377–382.
Söhnel, O., Mullin, J.W., 1988. Interpretation of crystallization induction periods. J. Colloid Interface Sci. 123 (1), 43–50.
Stockmann, G., Tollefsen, E., Skelton, A., Brüchert, V., Balic-Zunic, T., Langhof, J., Skogby, H., Karlsson, A., 2018. Control of a calcite inhibitor (phosphate) and temperature on ikaite precipitation in Ikka Fjord, Southwest Greenland. Appl. Geochem. 89, 11–22.
Suess, E., Balzer, W., Hesse, K.F., Müller, P.J., Ungerer, C.A., Wefer, G., 1982. Calcium carbonate hexahydrate from organic-rich sediments of the antarctic shelf: precursors of glendonites. Science (New York, N.Y.) 216 (4550), 1128–1131.
Tang, C.C., Thompson, S.P., Parker, J.E., Lennie, A.R., Azough, F., Kato, K., 2009. The ikaite-to-vaterite transformation: new evidence from diffraction and imaging. J. Appl. Crystallogr. 42 (2), 225–233.
Tlili, M.M., Amor, M.B., Gabrielli, C., Joiret, S., Maurin, G., Rousseau, P., 2002. Characterization of CaCO3 hydrates by micro-Raman spectroscopy. J. Raman Spectrosc. 33 (1), 10–16. https://doi.org/10.1002/jrs.806.
Tollefsen, E., Stockmann, G., Skelton, A., Mörth, C.-M., Dupraz, C., Sturkell, E., 2018. Chemical controls on ikaite formation. Mineral. Mag. 82 (5), 1119–1129.
Tollefsen, E., Balic-Zunic, T., Mörth, C.-M., Brüchert, V., Lee, C.C., Skelton, A., 2020. Ikaite nucleation at 35 °C challenges the use of glendonite as a paleotemperature indicator. Sci. Rep. 10 (1), 1–10.
Verdoes, D., Kashchiev, D., van Rosmalen, G.M., 1992. Determination of nucleation and growth rates from induction times in seeded and unseeded precipitation of calcium carbonate. J. Cryst. Growth 118 (3–4), 401–413.
Zaoui, A., Sekkal, W., 2014. Mechanisms behind the ikaite-to-calcite phase transformation from molecular dynamics calculations. Geoderma 235-236, 329–333.
Zou, Z., Bertinetti, L., Habraken, W.J.E.M., Fratzl, P., 2018. Reentrant phase transformation from crystalline ikaite to amorphous calcium carbonate. CrystEngComm 20 (21), 2902–2906.